Check for updates

Liquid Crystals Hot Paper

How to cite: *Angew. Chem. Int. Ed.* **2022**, *61*, e202203447
International Edition: doi.org/10.1002/anie.202203447
German Edition: doi.org/10.1002/ange.202203447

Tetrahedral Liquid-Crystalline Networks: An A15-Like Frank–Kasper Phase Based on Rod-Packing

Changlong Chen[+], Marco Poppe[+], Silvio Poppe, Matthias Wagner, Carsten Tschierske, and Feng Liu**

Abstract: The $Pm\bar{3}n$ cubic and other low-symmetry Frank–Kasper phases are known to be formed by soft spheres, ranging from metals to block copolymer micelles and colloidal nanoparticles. Here, we report a series of X-shaped polyphiles composed of sticky rods and two non-symmetric branched side-chains, which self-assemble into the first example of a cubic liquid-crystalline phase representing a tetrahedral network of rods with a $Pm\bar{3}n$ lattice. It is the topological dual to the Weaire–Phelan foam, being the Voronoi tessellation of the A15 sphere packing, from which this network is obtained by Delaunay triangulation.

Molecular self-assembly leads to multifunctional soft materials with nanoscopic and mesoscopic structures that provide promising properties for applications.[1] Broadening those future potential applications motivates studies of the fundamental principles of bottom-up self-assembly leading to ever more complex structures based on a delicate balance of non-covalent interactions[2] and geometric frustration.[3] Self-assembly of soft spherical or almost spherical molecules,[2,4] polymers,[5] aggregates,[6] micelles[7] and nanoparticles,[8] have been intensively investigated in recent decades. Uniform hard spheres are known to provide dense packing in simple body-centered cubic (BCC) and hexagonally closed (HCP) packings,[9] whereas soft spheres provide a series of more complex modes of self-assembly.[6a,10] The most common soft sphere packing is the A15 cubic phase with a $Pm\bar{3}n$ lattice shown in Figure 1a.[5a,6,7,10a] In the unit cell, two spheres occupy the center and the corners and six as pairs are on the faces. The formation of this structure, being composed of two different kinds of micelles in ratio 2:6 is nowadays understood as the result of the deformation of the soft spheres into Voronoi polyhedra[11] (dodecahedra in the center and at the corners and tetradecahedra on the faces, see Figure 1b), which minimizes the interfacial area between the soft spheres.[10]

The cubic $Pm\bar{3}n$ phase belongs to the Frank–Kasper (FK) phases,[12] i.e. a class of tetrahedrally close packed (TCP) structures which were firstly introduced for intermetallic compounds and more recently observed in self-assembled soft-matter structures.[5a,7d]

In contrast to sphere packings, the dense packing of molecular or supramolecular rods is mainly associated with the development of orientational order by parallel alignment and formation of nematic and lamellar liquid-crystalline (LC) phases.[13] Formation of other more complex structures requires either steric frustration, leading to bicontinuous cubic phases by network formation,[2a,14] chirality providing helical order between the rods,[1c,d,2b] or low density rod-packings.[15] The latter are supported by sticky ends, as

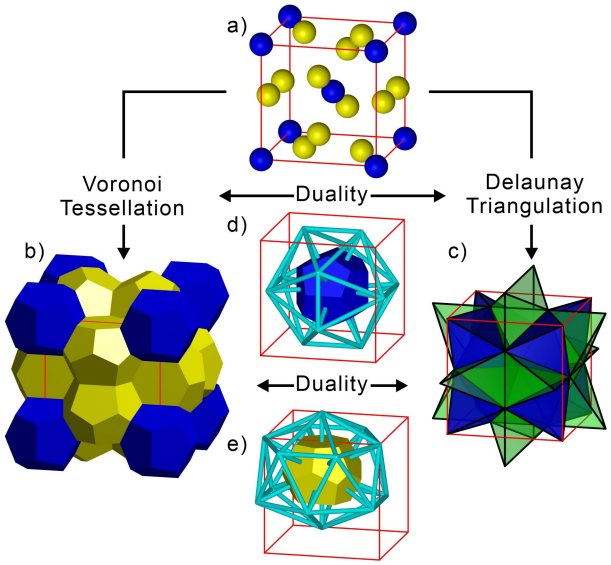

Figure 1. Packing modes in the Cub/$Pm\bar{3}n$ lattice: a) Positions of the spheroids in a unit cell; b) Weaire–Phelan foam by Voronoi tessellation (VT) for sphere packings; c) tetrahedral network by Delaunay triangulation (DT) for rod packings; d) and e) duality between the VT and DT.

[*] C. Chen,[+] Prof. Dr. F. Liu
Shaanxi International Research Center for Soft Matter, State Key Laboratory for Mechanical Behaviour of Materials, Xi'an Jiaotong University
Xi'an 710049 (P. R. China)
E-mail: feng.liu@xjtu.edu.cn

Dr. M. Poppe,[+] Dr. S. Poppe, M. Wagner, Prof. Dr. C. Tschierske
Department of Chemistry, Martin Luther University Halle-Wittenberg
Kurt-Mothes Str. 2, 06120 Halle/Saale (Germany)
E-mail: carsten.tschierske@chemie.uni-halle.de

[+] These authors contributed equally to this work.

© 2022 The Authors. Angewandte Chemie International Edition published by Wiley-VCH GmbH. This is an open access article under the terms of the Creative Commons Attribution Non-Commercial License, which permits use, distribution and reproduction in any medium, provided the original work is properly cited and is not used for commercial purposes.

© 2022 The Authors. Angewandte Chemie International Edition published by Wiley-VCH GmbH

reported for molecular rods with glycerol ends self-assembling into LC phases representing polygonal honeycombs.[16] If the rod-density is reduced, then interpenetrating 3d-nets, such as the double gyroid (DG) and the double diamond (DD) type cubic LC phases can be found, where the rods are organized in bundles and interconnected to networks with the hydrogen bonded glycerols at the junctions.[2a,17] The low packing density is achieved by side-on attached flexible chains which fill the space between the networks.

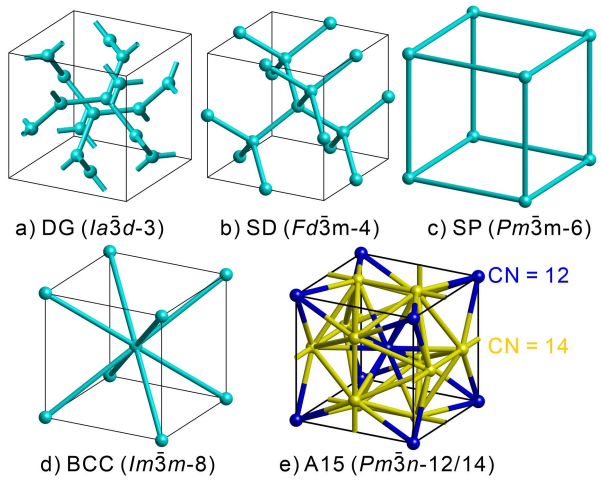

Figure 2. Different cubic lattices under discussion; the number(s) besides the space groups indicate(s) the CN of the junctions.

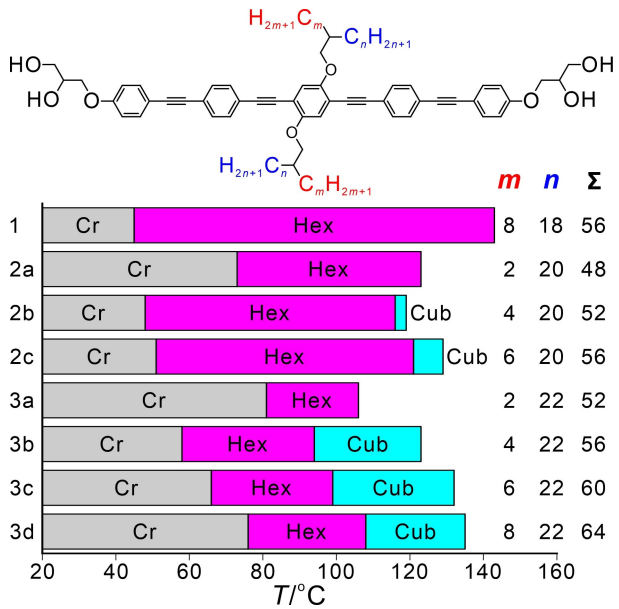

Figure 3. Molecular structure and phase transitions of compounds **1–3** upon cooling; abbreviations: Cr = crystalline state; Hex = hexagonal columnar phase with *p6mm* symmetry ($Col_{hex}/p6mm$), Cub = cubic phase with $Pm\bar{3}n$ symmetry (Cub/ $Pm\bar{3}n$); for DSCs, see Figure S1, for optical textures Figure S2 (Supporting Information), for numerical values, see Table S1 (Supporting Information); Σ is the total of all C-atoms in the side chains ($\Sigma = 2m + 2n + 4$); the synthesis of **3d** was previously reported.[21a]

The chain volume and chain distribution along the polyaromatic rods decides if honeycombs or networks are formed. In the networks a transition from interpenetrated double networks (DG,[17b] DD[17a]) to single networks (single diamond = SD,[18] single Plumber's Nightmare = SP[19] and a BCC lattice composed of open octahedral cells[20]) is observed upon side chain volume expansion (Figure 2). In this sequence the coordination numbers (CNs) of the junctions increases from 3 to 8. Here we report a new single network phase with $Pm\bar{3}n$ lattice and much higher CN (12,14).

This phase was found for oligo(phenylene-ethynylene) (OPE) based rod-like X-shaped bolapolyphiles with two branched chains,[20] each composed of two branches with different lengths and fixed at opposite sides of the central benzene ring (see Figure 3 and Table S1; for synthesis, see Supporting Information).

Compounds **1–3** with a total lateral chain volume (Σ, Figure 3) between 48 and 64 aliphatic carbons all form a birefringent hexagonal columnar LC phase ($Col_{hex}/p6mm$) with $a_{hex} = 4.14–4.21$ nm (Figures S2, S4 and Table S9), representing a triangular honeycomb (see Section S3.1 in Supporting Information for details), and being the topological dual of the hexagonal honeycomb (Figure S7).[22] Compound **1** with the smallest length difference between the branches ($n-m=10$), as well as compounds **2a** and **3a** with only a short ethyl branch and an especially large chain length difference ($n-m=18, 20$) show this phase exclusively, whereas all other compounds **2** and **3** with intermediate chain length differences form an additional optical isotropic LC phase as a high temperature phase (Figure 3). On cooling, the transition from the isotropic liquid to this isotropic mesophases is indicated by a small transition enthalpy of ≈ 0.5 kJ mol^{-1} (Table S1, Figure S1), a significant increase of viscosity and the emergence of sharp scatterings in the small angle X-ray scattering pattern (SAXS, see Figure 4a and S3), indicating the formation of a cubic LC phase.

Its SAXS pattern of the cubic LC phase can be indexed to a $Pm\bar{3}n$ space group with lattice parameters $a_{cub} = 8.6–8.8$ nm (see Table S8), corresponding to approximately twice the molecular length ($L_{mol} = 4.0–4.4$ nm between the ends of the glycerol groups). The diffuse wide-angle scattering (WAXS) with a maximum at ≈ 0.46 nm confirms a LC state without fixed positions for individual molecules (Figure S5). In the electron density (ED) maps reconstructed from the SAXS intensities (Figure 4b, for phase choice and other details, see Section S3.2, and Figures S8 and S9), the magenta-blue regions indicate the high-ED aggregations of the glycerols. Remarkably, the space between these aggregates is not uniform, but the polar spheroids are connected by cyan rods formed by the middle-ED OPEs. The 14-fold junctions on the faces of the unit cell are larger and oblate-shaped compared to the other smaller and almost spherical 12-fold junctions at the corners and in the center of the unit cell. Accordingly, a geometric model for simulation was constructed (Figure 4d), and the consistency of the intensity distributions of the SAXS peaks obtained in experiments and in simulation (Figure 4b–d and Section S3.3) supports a

© 2022 The Authors. Angewandte Chemie International Edition published by Wiley-VCH GmbH

15213773, 2022, 27, Downloaded from https://onlinelibrary.wiley.com/doi/10.1002/anie.202203447 by Fak-Martin Luther Universitats, Wiley Online Library on [11/09/2023]. See the Terms and Conditions (https://onlinelibrary.wiley.com/terms-and-conditions) on Wiley Online Library for rules of use; OA articles are governed by the applicable Creative Commons License

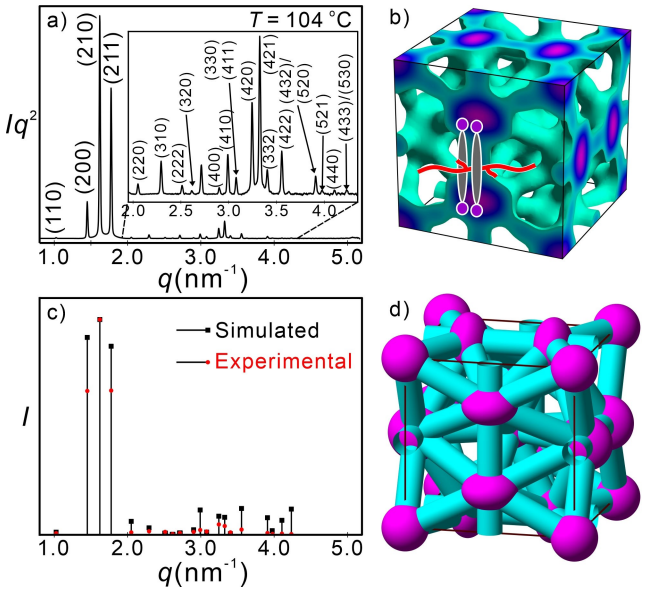

Figure 4. a) Powder SAXS diffractogram of **3b** and b) reconstructed ED map of the *Pm*$\bar{3}$*n* phase showing a tetrahedral network with aromatic bundles (cyan-blue) and glycerol junctions (blue-magenta); c) simulated intensities versus experimental results (corrected by multiplicities and Lorentz factor) and d) geometric model constructed from the proposed molecular packing for simulation. The aliphatic segments are omitted in (b) and (d) for clarity.

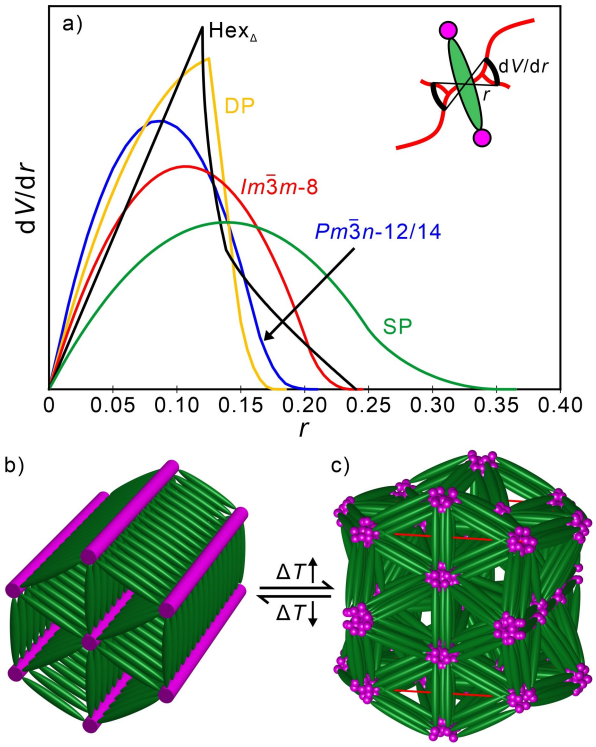

Figure 5. a) Radial volume distribution d*V*/d*r* curves of selected phases (see Figure 2 and Table S13 for the corresponding models); b), c) schematic models showing b) the triangular honeycomb with only one molecule in cross section of the walls (see Table S9), easily collapsing to c) the tetrahedral network of the *Pm*$\bar{3}$*n* phase (see also Figure S15).

tetrahedral network of molecular rod bundles (Figure 5c). The *Pm*$\bar{3}$*n* lattice is commonly found for the packing of soft spherical entities (A15 phase) which can be deformed to Voronoi polyhedra (Weaire–Phelan foam).[6a,10] As a dual to the Voronoi tessellation (VT) of the *Pm*$\bar{3}$*n* lattice there exists the Delaunay triangulation (DT) which fulfils the space with tetrahedra (see Figure 1b,c and the supporting animated gif-file).[11,23] This dense tetrahedral packing in a network with a *Pm*$\bar{3}$*n* lattice is here proposed for the self-assembly of the X-shaped compounds **2** and **3** with sticky ends, forming 12- and 14-fold junctions interconnecting the rod-bundles (*Pm*$\bar{3}$*n*-12/14). DT of the Weaire-Phelan foam separating the spheroidic aggregates in the *Pm*$\bar{3}$*n* lattice leads to three kinds of tetrahedra in the ratio of 16:24:6 composed of three kinds of bundles in a ratio of 6:24:24 (Table S11 and S12). The number of molecules in a unit cell is on average about ≈251, which are distributed among the 54 bundles, meaning there are on average about 5 molecules in the cross section of each bundle (Table S8). This is a reasonable value being only slightly smaller than the number in the bundles of the recently reported *Im*$\bar{3}$*m*-8 network phase (Figure 2d, 6 molecules).[20] The lengths of the bundles are $(\sqrt{4}, \sqrt{5}, \sqrt{6})/4 \times a_{cub}$, which corresponds to about 4.27–5.30 nm. While the larger inter-sphere distances compared to the molecular length are due to the high CN of the polar spheroidic nodes interconnecting the rods, the different bundle lengths are supported by the oblate shape of the polar spheroids at the faces. Alternative modes of rod-packing can be excluded as outlined in Sections S3.2 and S3.4 (Supporting Information).

The *Pm*$\bar{3}$*n* phase is formed between the triangular honeycomb and the isotropic liquid state on heating (see Figure 3 and Table S1). Thus, the formation of the *Pm*$\bar{3}$*n* lattice can be understood as a disruption of the triangular honeycomb of the Col_{hex} phase into a tetrahedral 3d network formed by triangular meshes due to the growing interface curvature between rigid polar and flexible apolar units (Figure 5b,c). Obviously, the triangulation of space is retained and transmitted at the phase transition from the honeycomb to the 3d network. But why is no alternative network with smaller CN formed?

The formation of the *Pm*$\bar{3}$*n* lattice (Figure 3) is obviously associated with the development of the lateral chain volume depending on the distance from the junction between chains and rods. In Figure 5a the radial volume distribution d*V*/d*r* curves[19,20,24] of different cubic phases with high CNs (6–14) are compared, also including the triangular honeycomb (Col_{hex}) for comparison. In the triangular honeycomb and the double network DP phase, there is an increase followed by a steep drop of the d*V*/d*r* curves due to the clashing of the chains in the limited available space between the cylinder walls or upon approaching the second network, respectively. For the non-interwoven single network cubic phases SP, *Im*$\bar{3}$*m*-8 and A15 (*Pm*$\bar{3}$*n*-12/14) (Figure 2c, d, e), there are smoother parabola-like d*V*/d*r* curves. These require a relatively large increase of the chain volume close

© 2022 The Authors. Angewandte Chemie International Edition published by Wiley-VCH GmbH

15213773, 2022, 27, Downloaded from https://onlinelibrary.wiley.com/doi/10.1002/anie.202203447 by Fak-Martin Luther Universitats, Wiley Online Library on [11/09/2023]. See the Terms and Conditions (https://onlinelibrary.wiley.com/terms-and-conditions) on Wiley Online Library for rules of use; OA articles are governed by the applicable Creative Commons License

to the core-chain junction which then smoothly decreases with further growing distance, in line with the branched chain architecture of compounds **2** and **3** with $m>2$. The actual chain volume distribution of the properly branched compounds **2** and **3** obviously fits best to the A15 ($Pm\bar{3}n$-12/14) phase whereas the competing SP and $Im\bar{3}m$-8 network phases would require longer chains (Figure 5a). As shown in Figure 3, there is also a competition between formation of triangular honeycombs and tetrahedra. Transition to the $Pm\bar{3}n$ phase requires a certain minimum chain volume to fill the tetrahedra ($\Sigma>48$ and elevated temperature) and a distinct minimum chain length ($n>18$) to reach the centers of the tetrahedra without excessive chain stretching. This requires branched chains with the correct chain volume and length difference between the two branches. On the other hand, too large chain volumes ($\Sigma\geq72$) lead to ordinary square honeycombs (without tilt of the molecules in the honeycomb walls).[21b,c]

Overall, it appears that the soft matter network phases based on self-assembly of rod-bundles with sticky ends can be divided into two types. Those with low CNs = 3–6, like those known for the bicontinuous cubic phases of lyotropic systems, and those with large CNs = 8–14, as typically observed for sphere packings (micellar cubic phases). The first group is determined by minimization of the interfaces separating the interpenetrating networks (DG, DD, DP). With growing lateral chain volume, the double networks are replaced by single networks which in turn require higher CNs = 4, 6, 8 (SD, SP, $Im\bar{3}m$-8) for proper space filling. The second type, reported herein, is based on tetrahedral rod-packings with spheres at the nodes (FK phases), leading to high CN junctions. As regular tetrahedra cannot form a periodic lattice in 3d space a geometric frustration arises which leads to the complex FK phases.[3] In the present case it provides the A15-like lattice composed of two types of junctions with CNs = 12,14, where deformation of the larger allows almost uniform distances between the surfaces of the polar spheroids at the junctions, in line with the fixed rod length of the involved molecules.

All previously known FK phases were formed by soft spheres and considered as governed by the minimization of the contact area of their Voronoi cells, minimizing their non-specific repulsion. In the case reported here, the $Pm\bar{3}n$ lattice is, *for the first time*, based on its dual, the close tetrahedral packing of bundles of molecular rods, being the DT of the Voronoi cells. The bundles are held together at the nodes by specific cohesive forces between the sticky glycerol ends. In this way the rods act as bonds interconnecting the spheroids at the junctions, and a competition between sphere packing and rod packing arises. In this respect there is also some relation to DNA coated nanoparticles arrays (spherical nucleic acids) where the repulsive interactions between the coronas is combined with attraction provided by the sticky single stranded DNA ends.[25] Thus, in both cases the bond-mediated interactions compete with the steric repulsion forces. Though for compounds **2** and **3**, it leads to the same $Pm\bar{3}n$ lattice as observed for soft sphere self-assembly, further tuning of the attractive and repulsive forces by molecular design can provide access to new LC FK phases and eventually even to liquid quasicrystalline phases based on tetrahedral networks. Moreover, a number of other complex LC network phases composed of rod-bundles can be envisaged, whose packing modes and symmetries differ from those observed for soft sphere packings[4–10] as well as those reported for lyotropic systems[7] and arrays of short DNA rods.[26]

Acknowledgements

This work was supported by the National Natural Science Foundation of China (No. 21761132033, 21374086) and the Deutsche Forschungsgemeinschaft (DFG, No. 392435074, 436494874—GRK 2670). The authors are grateful to Beamline BL16B1 at SSRF (Shanghai Synchrotron Radiation Facility, China) for providing the beamtime. Open Access funding enabled and organized by Projekt DEAL.

Conflict of Interest

The authors declare no conflict of interest.

Data Availability Statement

The data that support the findings of this study are available in the Supporting Information of this article.

Keywords: Cubic Liquid Crystals · Delaunay Triangulation · Frank–Kasper Phases · Self-Assembly · Tetrahedral Networks

[1] a) E. Busseron, Y. Ruff, E. Moulin, N. Giuseppone, *Nanoscale* **2013**, *5*, 7098–7140; b) T. Kato, J. Uchida, T. Ichikawa, T. Sakamoto, *Angew. Chem. Int. Ed.* **2018**, *57*, 4355–4371; *Angew. Chem.* **2018**, *130*, 4438–4455; c) H. K. Bisoyi, Q. Li, *Chem. Rev.* **2022**, *122*, 4887–4926; d) T. H. Lin, Y. Li, C. T. Wang, H. C. Jau, C. W. Chen, C. C. Li, H. K. Bisoyi, T. J. Bunning, Q. Li, *Adv. Mater.* **2013**, *25*, 5050–5054.

[2] a) C. Tschierske, *Angew. Chem. Int. Ed.* **2013**, *52*, 8828–8878; *Angew. Chem.* **2013**, *125*, 8992–9047; b) C. Tschierske, G. Ungar, *ChemPhysChem* **2016**, *17*, 9–26.

[3] J.-F. Sadoc, R. Mosseri, *Geometrical Frustration*, Cambridge University Press, Cambridge, **1999**.

[4] Z. B. Su, C. H. Hsu, Z. H. Gong, X. Y. Feng, J. B. Huang, R. M. Zhang, Y. Wang, J. L. Mao, C. Wesdemiotis, T. Li, S. Seifert, W. Zhang, T. Aida, M. J. Huang, S. Z. D. Cheng, *Nat. Chem.* **2019**, *11*, 899–905.

[5] a) K. D. Dorfman, *Macromolecules* **2021**, *54*, 10251–10270; b) M. T. Zhao, W. H. Li, *Macromolecules* **2019**, *52*, 1832–1842.

[6] a) G. Ungar, X. B. Zeng, *Soft Matter* **2005**, *1*, 95–106; b) H. J. Sun, S. D. Zhang, V. Percec, *Chem. Soc. Rev.* **2015**, *44*, 3900–3923.

[7] a) K. Fontell, *Colloid Polym. Sci.* **1990**, *268*, 264–285; b) V. Luzzati, R. Vargas, P. Mariani, A. Gulik, H. Delacroix, *J. Mol. Biol.* **1993**, *229*, 540–551; c) J. M. Seddon, N. Zeb, R. H. Templer, R. N. McElhaney, D. A. Mannock, *Langmuir* **1996**, *12*, 5250–5253; d) A. Jayaraman, M. K. Mahanthappa, *Langmuir* **2018**, *34*, 2290–2301.

© 2022 The Authors. Angewandte Chemie International Edition published by Wiley-VCH GmbH

15213773, 2022, 27, Downloaded from https://onlinelibrary.wiley.com/doi/10.1002/anie.202203447 by Fak-Martin Luther Universitats, Wiley Online Library on [11/09/2023]. See the Terms and Conditions (https://onlinelibrary.wiley.com/terms-and-conditions) on Wiley Online Library for rules of use; OA articles are governed by the applicable Creative Commons License

[8] a) D. Jishkariani, B. T. Diroll, M. Cargnello, D. R. Klein, L. A. Hough, C. B. Murray, B. Donnio, *J. Am. Chem. Soc.* **2015**, *137*, 10728–10734; b) M. A. Boles, M. Engel, D. V. Talapin, *Chem. Rev.* **2016**, *116*, 11220–11289; c) R. L. Marson, T. D. Nguyen, S. C. Glotzer, *MRS Commun.* **2015**, *5*, 397–406.
[9] L. T. Chen, C. Y. Chen, H. L. Chen, *Polymer* **2019**, *169*, 131–137.
[10] a) P. Ziherl, R. D. Kamien, *J. Phys. Chem. B* **2001**, *105*, 10147–10158; b) L. Athanasopoulou, P. Ziherl, *Soft Matter* **2017**, *13*, 1463–1471.
[11] A. Okabe, B. Boots, K. Sugihara, S. N. Chiu, *Spatial tessellations: Concepts and applications of Voronoi diagrams*, 2nd ed., Wiley, Chichester, **2000**.
[12] a) F. C. Frank, J. S. Kasper, *Acta Crystallogr.* **1958**, *11*, 184–190; b) F. C. Frank, J. S. Kasper, *Acta Crystallogr.* **1959**, *12*, 483–499.
[13] J. W. Goodby, P. J. Collings, H. Gleeson, P. Raynes, T. Kato, C. Tschierske, *Handbook of Liquid Crystals*, 2nd ed., Wiley-VCH, Weinheim, **2013**.
[14] a) H. T. Nguyen, C. Destrade, J. Malthéte, *Adv. Mater.* **1997**, *9*, 375–388; b) S. Kutsumizu, *Isr. J. Chem.* **2012**, *52*, 844–853.
[15] R. Chelakkot, R. Lipowsky, T. Gruhn, *Macromolecules* **2006**, *39*, 7138–7143.
[16] C. Tschierske, C. Nurnberger, H. Ebert, B. Glettner, M. Prehm, F. Liu, X. B. Zeng, G. Ungar, *Interface Focus* **2012**, *2*, 669–680.
[17] a) X. Zeng, M. Prehm, G. Ungar, C. Tschierske, F. Liu, *Angew. Chem. Int. Ed.* **2016**, *55*, 8324–8327; *Angew. Chem.* **2016**, *128*, 8464–8467; b) S. Poppe, C. Chen, F. Liu, C. Tschierske, *Chem. Commun.* **2018**, *54*, 11196–11199.
[18] X. Zeng, S. Poppe, A. Lehmann, M. Prehm, C. Chen, F. Liu, H. Lu, G. Ungar, C. Tschierske, *Angew. Chem. Int. Ed.* **2019**, *58*, 7375–7379; *Angew. Chem.* **2019**, *131*, 7453–7457.
[19] S. Poppe, X. H. Cheng, C. L. Chen, X. B. Zeng, R. B. Zhang, F. Liu, G. Ungar, C. Tschierske, *J. Am. Chem. Soc.* **2020**, *142*, 3296–3300.
[20] C. Chen, M. Poppe, S. Poppe, C. Tschierske, F. Liu, *Angew. Chem. Int. Ed.* **2020**, *59*, 20820–20825; *Angew. Chem.* **2020**, *132*, 21006–21011.
[21] a) M. Poppe, C. Chen, S. Poppe, F. Liu, C. Tschierske, *Commun. Chem.* **2020**, *3*, 70; b) M. Poppe, C. Chen, F. Liu, M. Prehm, S. Poppe, C. Tschierske, *Soft Matter* **2017**, *13*, 4676–4680; c) S. Poppe, M. Poppe, H. Ebert, M. Prehm, C. Chen, F. Liu, S. Werner, K. Bacia, C. Tschierske, *Polymers* **2017**, *9*, 471.
[22] T. C. Hales, *Discrete. Comput. Geom.* **2001**, *25*, 1–22.
[23] B. Delaunay, *Bull. Acad. Sci. URSS Cl. Sci. Math. Nat.* **1934**, *6*, 793–800.
[24] a) G. Ungar, Y. S. Liu, X. B. Zeng, V. Percec, W. D. Cho, *Science* **2003**, *299*, 1208–1211; b) X. H. Yao, L. Cseh, X. B. Zeng, M. Xue, Y. S. Liu, G. R. Ungar, *Nanoscale Horiz.* **2017**, *2*, 43–49.
[25] a) S. Angioletti-Uberti, B. M. Mognetti, D. Frenkel, *Phys. Chem. Chem. Phys.* **2016**, *18*, 6373–6393; b) R. J. Macfarlane, B. Lee, M. R. Jones, N. Harris, G. C. Schatz, C. A. Mirkin, *Science* **2011**, *334*, 204–208.
[26] Y. Tian, J. R. Lhermitte, L. Bai, T. Vo, H. L. L. Xin, H. L. Li, R. P. Li, M. Fukuto, K. G. Yager, J. S. Kahn, Y. Xiong, B. Minevich, S. K. Kumar, O. Gang, *Nat. Mater.* **2020**, *19*, 789–796.

Manuscript received: March 6, 2022
Accepted manuscript online: April 25, 2022

© 2022 The Authors. Angewandte Chemie International Edition published by Wiley-VCH GmbH

15213773, 2022, 27, Downloaded from https://onlinelibrary.wiley.com/doi/10.1002/anie.202203447 by Fak-Martin Luther Universitats, Wiley Online Library on [11/09/2023]. See the Terms and Conditions (https://onlinelibrary.wiley.com/terms-and-conditions) on Wiley Online Library for rules of use; OA articles are governed by the applicable Creative Commons License